Impaired hippocampal rhythmogenesis in a mouse model of mesial temporal lobe epilepsy

Tamar Dugladze*, Imre Vida†, Adriano B. Tort‡, Anna Gross†, Jacub Otahal§, Uwe Heinemann*, Nancy J. Kopell‡¶, and Tengis Gloveli*¶

*Institute of Neurophysiology, Charité Universitätsmedizin Berlin, Tucholskystrasse 2, D-10117 Berlin, Germany; †Institute of Anatomy and Cell Biology, University of Freiburg, Albertstrasse 17, D-79104 Freiburg, Germany; ‡Department of Mathematics and Center for Biodynamics, Boston University, 111 Cummington Street, Boston, MA 02215; and §Department of Developmental Epileptology, Institute of Physiology, Academy of Sciences of the Czech Republic, 142 20 Prague, Czech Republic

Contributed by Nancy J. Kopell, September 12, 2007 (sent for review April 22, 2007)

Mesial temporal lobe epilepsy (mTLE) is one of the most common forms of epilepsy, characterized by hippocampal sclerosis and memory deficits. Injection of kainic acid (KA) into the dorsal hippocampus of mice reproduces major electrophysiological and histopathological characteristics of mTLE. In extracellular recordings from the morphologically intact ventral hippocampus of KA-injected epileptic mice, we found that theta-frequency oscillations were abolished, whereas gamma oscillations persisted both *in vivo* and *in vitro*. Whole-cell recordings further showed that oriens-lacunosum-moleculare (O-LM) interneurons, key players in the generation of theta rhythm, displayed marked changes in their intrinsic and synaptic properties. Hyperpolarization-activated mixed cation currents (Ih) were significantly reduced, resulting in an increase in the input resistance and a hyperpolarizing shift in the resting membrane potential. Additionally, the frequency of spontaneous excitatory postsynaptic currents (sEPSCs) was increased, indicating a stronger excitatory input to these neurons. As a consequence, O-LM interneurons increased their firing rate from theta to gamma frequencies during induced network activity in acute slices from KA-injected mice. Thus, our physiological data together with network simulations suggest that changes in excitatory input and synaptic integration in O-LM interneurons lead to impaired rhythmogenesis in the hippocampus that in turn may underlie memory deficit.

in vitro | interneurons | oscillations | patch–clamp | *in vivo*

Mesial temporal lobe epilepsy (mTLE) is the most common form of focal epilepsy in adults, and it is the most common therapy-resistant seizure disorder (1). Memory problems are common in human and animal models of mTLE, but the mechanisms are unclear (2–4). Several animal models have been developed to investigate the cellular and network mechanisms of epilepsy. Kainic acid (KA) causes an epileptic syndrome similar to human mTLE, with sclerosis and structural reorganization in the mesial temporal lobe, spontaneous seizures, and significant deficits in spatial learning and memory (5–7). Although impaired hippocampal rhythmogenesis resulting from changes in anatomical connectivity, as well as intrinsic and synaptic properties of neuronal circuits, could contribute to the memory deficits, the behavioral consequences of KA have so far been interpreted solely as a consequence of the KA-induced seizures (7).

It has been proposed that mTLE is associated with an alteration in the balance of inhibition and excitation in hippocampal networks. Consistent with this hypothesis, impressive changes in the number and connectivity of various types of GABAergic inhibitory interneurons, as well as in the expression of $GABA_A$ and $GABA_B$ receptors, has been observed both in mTLE patients and in experimental animals (8–10). However, recent experimental studies revealed that reduction of inhibition in epilepsy is not uniform but shows a characteristic spatial distribution over the surface of principal cells. Whereas inhibitory input onto the dendrites of the hippocampal pyramidal cells is reduced, it is preserved on the perisomatic domain (10–12). Furthermore, imbalance of inhibition and excitation may emerge in the temporal domain. Interneurons fire rhythmically, phase-locked to network oscillations at theta (4–12 Hz) or gamma frequencies (30–80 Hz). The activity of various types of interneurons results in precisely controlled rhythmic fluctuations in the excitability of principal cells at multiple time scales (13). Changes in the finely tuned spatiotemporal pattern of inhibition can lead to an altered rhythmogenesis in the epileptic network. In fact, it has been recently reported that the power of theta-frequency oscillations, prominent both in rodents and humans during spatial navigation and memory tasks (14–17), is reduced in KA-injected epileptic mice (18). The altered oscillatory activity in the hippocampal network may in turn influence the storage of new memory traces and the behavioral performance in hippocampus-dependent tasks such as spatial navigation (14).

In the present study, we have investigated rhythmogenesis in mTLE in chronic epileptic mice after a unilateral injection of KA into the dorsal hippocampus by using a combined electrophysiological, neuroanatomical, and computational approach. Our results show that theta activity is absent, whereas gamma activity persists in the CA3 region of the ventral hippocampus of epileptic mice both *in vivo* and *in vitro*. Analysis of cellular mechanisms revealed that the discharge frequency of the dendrite-inhibiting oriens-lacunosum-moleculare (O-LM) interneuron, a key player in the generation of theta rhythm (19), has changed from the theta to the gamma band. The change in the firing frequency is directly related to an increased excitatory input in these interneurons. Thus, our data indicate that a change in the synaptic and firing properties of dendrite-inhibiting interneurons leads to impaired rhythmogenesis in hippocampal networks of this model of mTLE.

Results

The Cellular Structure Is Preserved in the Ventral Hippocampus of the KA-Injected Mice. Morphological analysis 3–4 weeks after the injection of KA revealed profound structural alterations in the dorsal hippocampus. In the CA1, CA3c, and the hilar regions, diminished immunoreactivity for the neuron-specific marker NeuN indicated a significant loss of neurons, and an enhanced immunostaining for the glial-specific marker glial fibrillary acidic protein (GFAP) further reflected a reactive gliosis. In the dentate gyrus, granule cells showed hypertrophy and dispersion

Author contributions: T.D. and T.G. designed research; T.D., A.B.T., and T.G. performed research; T.D., I.V., A.B.T., A.G., J.O., U.H., N.J.K., and T.G. analyzed data; and I.V., N.J.K., and T.G. wrote the paper.

The authors declare no conflict of interest.

Abbreviations: EPSC, excitatory postsynaptic current; Ih, hyperpolarization-activated mixed cation currents; IR, input resistance; KA, kainic acid; LFP, local field potential; mEPSC, miniature EPSC; MP, membrane potential; mTLE, mesial temporale lobe epilepsy; O-LM, oriens-lacunosum-moleculare; sEPSC, spontaneous EPSC.

¶To whom correspondence may be addressed. E-mail: tengis.gloveli@charite.de or nk@math.bu.edu.

This article contains supporting information online at www.pnas.org/cgi/content/full/0708301104/DC1.

[supporting information (SI) Fig. 5*B*; refs. 6 and 20]. These morphological changes were restricted to the injected dorsal parts, whereas the ventral hippocampus appeared to be structurally intact (SI Fig. 5 *A* and *B*; ref. 8).

Previous studies showed that the anatomical alterations are not limited to the principal cell population but also affect GABAergic interneurons (8). In the present investigation, we have focused on the neurochemical marker somatostatin, a neuropeptide expressed by O-LM cells, a type of dendrite-inhibiting interneuron involved in the generation of theta activity (19). In agreement with previous data, our results showed that immunostaining of somata and axons for this marker were strongly reduced in the dorsal hippocampus (data not shown), whereas in the ventral hippocampus the immunostaining pattern appeared to be largely unaltered (SI Fig. 5 *C* and *D*). Similar to the distribution in control animals, somata of somatostatin-immunopositive interneurons were primarily found in the stratum oriens, pyramidale, and lucidum of the ventral CA3 area. Quantitative analysis further showed that the density of the interneurons was not reduced in this area in KA-injected animals [440 ± 54 per mm^3 (three control mice) vs. 514 ± 44 per mm^3 (four epileptic mice)]. Similarly, no significant change in the density of the interneurons was observed in the CA1 area of the ventral hippocampus in KA-injected animals [554 ± 76 per mm^3 (three control mice) vs. 536 ± 138 per mm^3 (four epileptic mice)]. Thus, our immunocytochemical results suggest that the cellular structure, including somatostatin-immunoreactive interneurons, is preserved in the ventral circuits of the KA-injected hippocampus.

Theta-Frequency Oscillations Are Absent in the Ventral Hippocampus of KA-Injected Mice both *in Vivo* and *in Vitro*. To identify electrophysiological alterations after KA injection, we carried out electroencephalogram recordings from the hippocampus of freely moving control (Fig. 1*A1* and *A2*) and epileptic mice (Fig. 1 *B1* and *B2*). Chronic recordings from the dorsal hippocampus showed recurrent seizure activity in mice between 3–4 weeks after the injection (n = 5, data not shown; ref. 6). These paroxysmal discharges lasted 12–25 s (mean: 18.8 ± 2.1 s, n = 5).

In the ventral hippocampus, no seizures were detected in the KA-injected mice (n = 6), but electroencephalogram activity was less regular and had a larger amplitude than in control mice (Fig. 1*B1*), with sporadically occurring spikes and sharp waves (mean frequency: 0.6 ± 0.1 Hz). Spectral analysis of the *in vivo* recordings during exploratory behavior revealed further differences between control and epileptic mice. In control animals, power spectra showed two peaks corresponding to theta (4–8 Hz) and gamma frequencies (30–80 Hz) (Fig. 1*A2*), reflecting a nested theta–gamma rhythm associated to explorative behavior (21); in KA-injected animals, the peak in the theta-frequency band diminished, whereas the peak in the gamma range persisted in the spectra (Fig. 1*B2*). In summary, the *in vivo* data revealed seizure activity in dorsal hippocampus and an altered rhythmogenesis in the ventral hippocampal circuits of KA-injected mice.

To analyze the changes in oscillatory pattern generation in the ventral hippocampus, we continued our investigations *in vitro* by performing dual extracellular recordings from acute coronal hippocampal slices (22). In slices from control animals, a nested theta–gamma rhythm was generated in the CA3 area after bath application of a low concentration of KA (400 nM; n = 8; Fig. 1*C1*) or carbachol (20 μM; n = 6; data not shown). The power spectra of the oscillations in these slices showed two peaks corresponding to the two frequency bands (Fig. 1*C2*). In slices from KA-injected mice, bath application of the drugs induced no theta activity but large-amplitude, gamma-frequency oscillations [for KA: control, $3.4 \times 10^{-4} \pm 0.5 \times 10^{-4}$ mV^2/Hz, n = 8; epileptic, $9.3 \times 10^{-4} \pm 1.3 \times 10^{-4}$ mV^2/Hz, n = 12, $P < 0.05$ (Fig. 1 *D1* and *D2*); and for carbachol: control, $2.9 \times 10^{-4} \pm 0.3 \times 10^{-4}$ mV^2/Hz, n = 6; epileptic, $7.2 \times 10^{-4} \pm 0.8 \times 10^{-4}$ mV^2/Hz, n = 6, $P < 0.05$]. The power and coherence of gamma activity decreased rapidly along the CA3 area in the ventral direction in these slices (Fig. 1 *E* and *F*). Thus, the *in vitro* data confirmed the lack of theta rhythm and revealed altered properties of gamma activity in slices from KA-injected mice, further pointing to an altered rhythmogenesis in the ventral hippocampus of these animals.

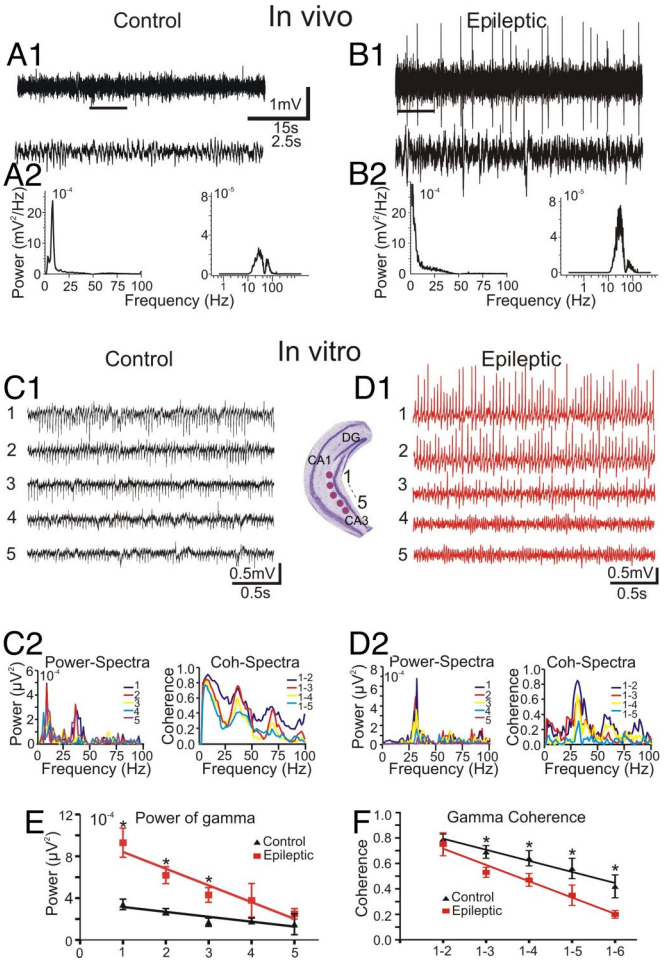

Fig. 1. *In vivo* and *in vitro* field potential recordings from area CA3 of the ventral hippocampus of control and epileptic animals. (*A1–B2*) Representative electroencephalogram recordings from the ventral hippocampus of control and epileptic freely moving mice. (*A1* and *A2*) Typical theta activity (*A1*) (peak frequency, 7.3 Hz) (*A2 Left*) in control mice during an exploratory behavior. (*B1* and *B2*) Theta oscillatory activity (*B1*) was no longer seen in epileptic mice (*B2 Left*) during a chronic phase of TLE. (*A1* and *B1*) Lower traces show time-expanded views of the region indicated by the bars in upper traces. (*A2 Right* and *B2 Right*) Band-path (30–80 Hz) filtered recordings from both animal groups unmasked the gamma-oscillatory activity (peak frequencies: 37 Hz and 39 Hz, in control and epileptic mice, respectively). (*C1*) Simultaneous expression of gamma- and theta- frequency oscillations in the control coronal slices after bath-applied KA (400 nM). (*Inset*) Schematic illustration of a coronal slice with the recording sites in ventral hippocampal CA3 region. (*C2*) (*Left*) Power–spectral density plots present two clear peaks at theta- (8 Hz) and gamma- (37 Hz) frequency range. (*Right*) Coherence spectra obtained from different recording sites. (*D1* and *D2*) In marked contrast to control, coronal slices from epileptic mice demonstrate gamma, but not theta activity. (*E*) Averaged power–spectral density for gamma-oscillatory activity obtained from different recording sites. (*F*) Averaged gamma-coherence patterns during the network oscillations in the coronal slices (n = 8).

O-LM Interneuron-Discharge Frequency Shifts from the Theta to the Gamma Range in KA-Injected Mice. To identify cellular mechanisms underlying the changes in rhythmogenesis, we continued by performing whole-cell patch–clamp recordings from interneurons

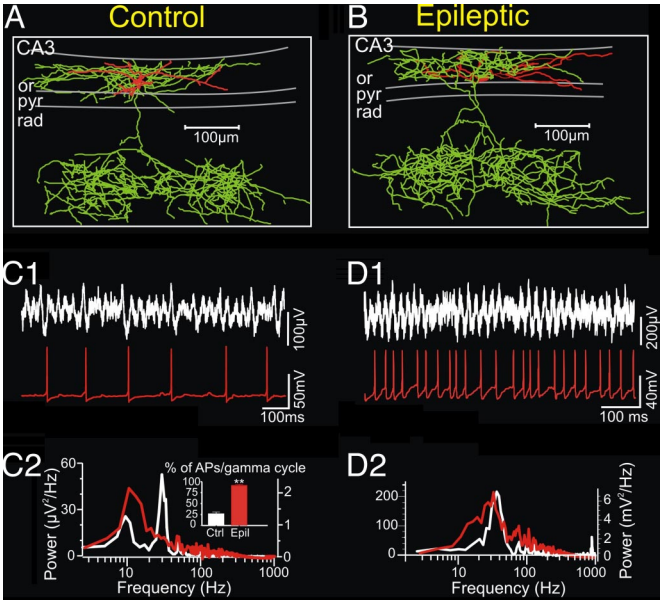

Fig. 2. Morphological and electrophysiological characterization of O-LM interneurons from control and epileptic coronal slices. (*A* and *B*) Neurolucida reconstruction of biocytin-filled O-LM cells in area CA3 of ventral hippocampus from control (*A*) and epileptic (*B*) animals. The soma and dendrites are drawn in red, whereas the axon is in green. Note that the axon collaterals in stratum lacunosum-moleculare demonstrate a tendency to form the separate axonal clusters along the coronal axis in both cells. (*C1* and *D1*) Representative concomitant field potential and whole-cell current–clamp recordings in coronal slices after induction of oscillatory activity by bath-applied KA (400 nM). (*C1* and *C2*) Control O-LM cells show the low-frequency discharges at the theta-frequency range (*C1*) during simultaneous field theta- and gamma-frequency oscillations (*C2*). (*D1*) In contrast to control cells, O-LM interneurons from epileptic mice demonstrate significantly higher action-potential firing at a mean gamma-frequency range during the field gamma-frequency oscillations. (*C2* and *D2*) Corresponding power spectra (60-s epoch) from field (white) and current clamp (red) recordings.

during induced population activity *in vitro*. We concentrated on somatostatin-containing O-LM interneurons because of their key role in the generation of theta activity (19, 23). Morphological analysis of biocytin-filled O-LM cells revealed no differences between control and experimental groups ($n = 9$ and $n = 12$, respectively; Fig. 2 *A* and *B*), further confirming the structural preservation of the ventral hippocampus in KA-injected mice.

During network activity induced by puff application of 1 mM KA in control slices, O-LM interneurons fired at a low frequency (Fig. 2*C*). Their average firing probability in a gamma cycle was 26.2 ± 4.8% ($n = 6$), and the mean firing frequency was in the theta range (8.6 ± 4.4 Hz). In slices from epileptic animals, O-LM cells showed a different activity pattern. They discharged on nearly each gamma cycle of the extracellular field oscillations (90.9 ± 3.1%, $n = 6$), and their mean discharge frequency was shifted to the gamma range (33.8 ± 2.6 Hz; Fig. 2 *D1* and *D2*).

Altered Intrinsic Properties in O-LM Interneurons in KA-Injected Mice. To clarify the mechanisms underlying differences in the firing pattern during gamma-frequency oscillations, we next investigated the intrinsic properties of O-LM cells. The resting membrane potential (MP) of the interneurons from KA-treated mice was more hyperpolarized (−61.8 ± 1.6 mV, $n = 9$ vs. −56.0 ± 1.1 mV, $n = 8$) and the input resistance (IR) was higher (231.1 ± 14.9 MΩ vs. 186.7 ± 19.9 MΩ, $P < 0.05$) than those from control animals. The apparent membrane time constant of O-LM cells in epileptic animals was slightly, but not significantly, higher (19.9 ± 2.0 ms vs. 15.7 ± 2.8 ms, $P = 0.1$).

Another difference was detected when the firing properties of cells from two groups current-clamped at the same MP (−60 mV) were compared during depolarizing current injection (see SI Fig. 6 *A* and *B*). The O-LM cells from epileptic mice exhibit higher firing frequencies in response to small depolarizing current pulses (≤100 pA).

Because membrane-intrinsic oscillatory properties (24) of O-LM cells are an important determinant of their discharge pattern, we tested whether these properties changed. Interneurons, depolarized near spike threshold by positive current injection (usually <50 pA), showed a MP oscillation in the theta band in both control and epileptic slices. The oscillatory frequencies were 6.9 ± 1.2 Hz in epileptic ($n = 8$) and 6.8 ± 1.8 Hz in control O-LM cells ($n = 5$, $P > 0.05$).

Reduced Hyperpolarization-Activated Mixed Cation Currents (Ih) in O-LM Interneurons in KA-Injected Mice. A possible explanation for these combinations of changes is a reduction in Ih in the interneurons (25, 26). To test this hypothesis, we applied hyperpolarizing current pulses to the cells held at −60 mV. Small hyperpolarizing pulses (≤100 pA) elicited significantly smaller sag potential in epileptic cells compared with control cells [3.4 ± 0.6 mV (seven epileptic cells) vs. 5.5 ± 0.6 mV (seven control cells); $P < 0.05$; see SI Fig. 6 *C1* and *D*]. A corresponding result was obtained in voltage–clamp mode in the presence of Tetrodotoxin (TTX) and Ba^{2+}. The inward current activated by small hyperpolarizing voltage steps (from −50 to −90 mV) was significantly smaller in epileptic than in control O-LM cells (50.8 ± 4.9 pA vs. 74.6 ± 9.5 pA, respectively, $n = 5$ for each group, $P < 0.05$). We next applied the Ih blocker ZD7288 to O-LM cells from control and epileptic mice (data not shown). The residual currents measured in the presence of ZD7288 at voltage changed from −50 to −90 mV were similar (control, 211 ± 33 pA, $n = 3$; epileptic, 230 ± 35 pA, $n = 3$, $P > 0.05$). These results indicate that different IR in O-LM cells from control and epileptic mice depend on a ZD7288-sensitive Ih current. Thus, our data revealed a reduction in the Ih that resulted in an increased IR and a hyperpolarized resting MP in O-LM interneurons from KA-injected mice.

Increased Excitatory Input to O-LM Interneurons in KA-Injected Mice. To evaluate glutamate receptor-mediated synaptic excitation in O-LM cells, we recorded spontaneous excitatory postsynaptic currents (sEPSCs) in slices from control ($n = 6$ cells) and epileptic mice ($n = 9$ cells, Fig. 3) at a holding potential close to the reversal potential of $GABA_A$ receptor-mediated postsynaptic currents (−70 mV). Analysis of sEPSCs showed that their mean frequency was increased to 173.3% in interneurons from KA-injected animals in comparison with controls (28.6 ± 1.2 Hz vs. 16.5 ± 2.6 Hz, $P < 0.01$; Fig. 3 *A1*, *B1*, and *C*). Whereas decay time was slightly, but not significantly, increased (8.1 ± 0.9 ms vs. 6.4 ± 0.9 ms, $P > 0.05$), rise time and amplitude were similar to controls (1.12 ± 0.2 ms vs. 1.12 ± 0.1 ms and 36.7 ± 1.3 pA vs. 38.7 ± 4.4 pA, in epileptic and control cells, respectively, $P > 0.05$). Next, we evaluated the frequency of miniature EPSCs (mEPSCs) (Fig. 3 *A1*, *B1*, and *D*). In contrast to sEPSCs, the mean frequency of mEPSCs showed a decrease in epileptic cells (3.2 ± 0.3 Hz, $n = 5$) in comparison with that in control mice (5.4 ± 1.2 Hz, $n = 4$, $P < 0.05$). Although there was a significant increase in the decay time-constant of mEPSCs in epileptic mice [10.4 ± 0.8 ms (in five epileptic mice) vs. 7.6 ± 0.7 ms (in four control cells), $P < 0.05$], the rise time and peak amplitude of mEPSCs did not differ [1.55 ± 0.2 ms and 23.1 ± 1.6 pA, $n = 5$ (epileptic) vs. 1.60 ± 0.2 ms and 24.7 ± 1.3 pA, $n = 4$, $P > 0.05$ (control); Fig. 3]. These results indicate that the increased sEPSC frequency is a consequence of enhanced activity of principal cells. Moreover, the decreased frequency of mEPSC may reflect a loss of some excitatory synapses onto O-LM cells in the ventral hippocampus in epileptic animals.

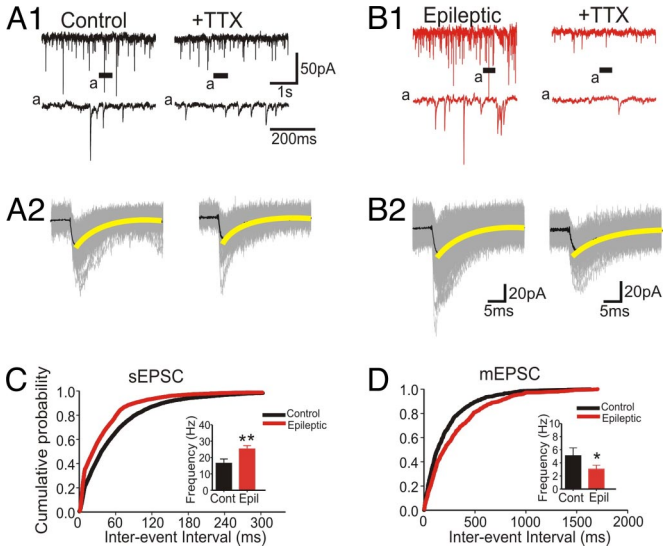

Fig. 3. sEPSCs and mEPSCs of O-LM cells recorded in slices from a control and chronic epileptic mice. (*A1* and *B1*) *Lower* traces show time-expanded views of the regions indicated by the bars under *Upper* traces; see ''a'' in both. (*A2* and *B2*) Two hundred and 70 individual traces for sEPSCs and mEPSCs, respectively, are shown in gray, and superimposed averaged potentials are shown in black. Decay of the averaged EPSPs in O-LM cells from both groups is well fitted by a single exponential function (yellow). Whole-cell recordings were obtained at the reversal potential of GABAergic events (≈−70 mV). (*C* and *C Inset*) The cumulative probability plot of the interevent interval of spontaneous events from epileptic O-LM cells was shifted to the left (red) (*C*), indicating an increased frequency of excitatory currents ($P < 0.01$) (*Inset*). (*D* and *D Inset*) The interevent interval of mEPSCs was shifted to the right (*D*) as result of decreased frequency in epileptic O-LM interneurons (*Inset*).

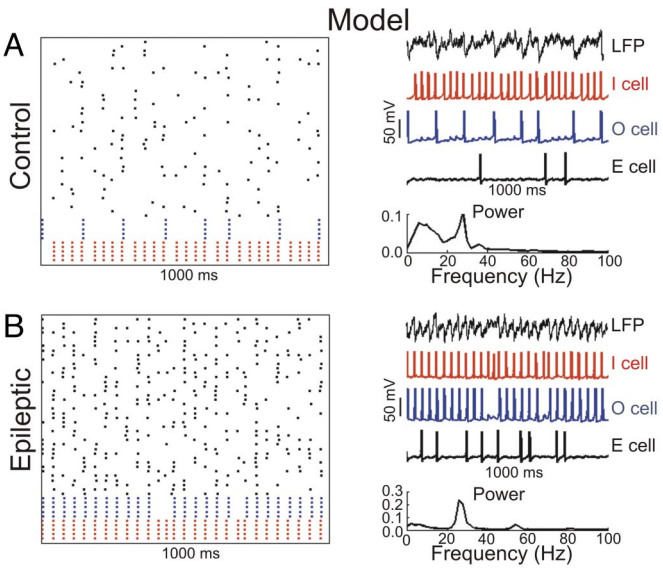

Fig. 4. Simulation of model CA3 networks. (*A*) (*Left*) Representative rastergram of a control network showing spike times of 40 E cells (black), 5 O cells (blue), and 5 I cells (red) during 1,000 ms of simulation. Note that the E cells spike sparsely and randomly (mean frequency of 3.39 ± 0.24 Hz), whereas I cells spike in every gamma cycle, and O cells spike at theta frequency. (*Right Upper*) Model LFP (arbitrary units) and sample voltage traces of each cell type for the same period of simulation shown in *Left*. (*Right Lower*) Power-spectrum analysis of model LFP (arbitrary units) evidencing coexistence of theta and gamma oscillations. (*B*) In the epileptic network, E cells present an increase in their spike activity (mean frequency of 8.66 ± 0.41 Hz), and O cells spike in most of gamma cycles. The power-spectrum analysis of the model LFP evidences a loss of theta oscillation and an increase in gamma power (note change in the scale). For the epileptic network, the E cell drive was increased from 22.5 μA/cm^2 to 25.5 μA/cm^2, and O cells' Ih maximal conductance was reduced from 7 mS/cm^2 to 4 mS/cm^2 (see *SI Appendix 2* for all model parameters).

In a complementary set of experiments, the synaptic inhibition of O-LM cells was examined. The properties of spontaneous inhibitory postsynaptic currents (sIPSCs) were not different in control ($n = 6$) and experimental ($n = 5$) animals (frequency, 5.6 ± 1.5 Hz vs. 7.9 ± 2.3 Hz; amplitude: 30.4 ± 3.4 pA vs. 34.6 ± 3.9 pA; rise time, 1.1 ± 0.04 ms vs. 1.1 ± 0.11 ms; decay time, 7.0 ± 0.8 ms vs. 8.8 ± 1.4 ms, $P > 0.05$). Likewise, no differences were detected in the properties of miniature inhibitory postsynaptic currents (mIPSCs) between the control and epileptic mice (frequency, 2.8 ± 1.1 Hz vs. 3.9 ± 0.5 Hz; amplitude, 18.3 ± 1.9 pA vs. 23.7 ± 3.8 pA; rise time, 1.9 ± 0.1 ms vs. 1.9 ± 0.1 ms; decay time, 13.5 ± 0.7 ms vs. 15.3 ± 0.6, $n = 4$ and $n = 3$, respectively, $P > 0.05$).

In summary, our data suggest that the O-LM cells in epileptic mice receive an enhanced excitatory and an unchanged inhibitory input.

Enhanced Activity of Pyramidal Cells in KA-Injected Mice. Because O-LM interneurons receive their excitatory drive primarily from pyramidal cells (27), we investigated whether the increased synaptic input and firing frequency of those interneurons were consequences of an enhanced activity of pyramidal cells. Recordings from pyramidal cells during network oscillation *in vitro* showed that these cells discharged at a higher frequency in slices from KA-injected mice (8.5 ± 2.3 Hz, $n = 4$, $P < 0.05$) than in control mice (3.4 ± 0.8 Hz, $n = 6$).

We next evaluated the firing properties of these cells in pharmacologically naive slices to gain insight into the mechanisms underlying their enhanced activity. Similar to O-LM neurons, pyramidal cells from epileptic mice exhibited significantly higher frequencies and a lower threshold for action potential generation in response to small (40–80 pA) depolarizing current injection (control, 0.2 ± 0.2 Hz and 1.2 ± 0.5 Hz, $n = 6$; epileptic, 2.9 ± 1.1 and 9.4 ± 2.4 Hz, $n = 7$, upon 40- and 80-pA current pulse given from −60 mV, $P < 0.05$).

Finally, we tested whether subthreshold oscillatory properties of pyramidal cells also changed in KA-injected animals. Pyramidal cells both in control and epileptic slices showed MP oscillations at theta frequencies (control, 6.8 ± 0.9 Hz, $n = 6$; epileptic, 7.5 ± 0.9 Hz, $n = 4$; $P > 0.05$) in response to depolarizing current pulses. Thus, the increased firing frequency of these cells was not caused by the changes in the intrinsic membrane oscillatory properties but by a reduced current threshold.

Model CA3 Epileptic Network Presents Loss of Theta Oscillations and Increase in Gamma Power. We next performed computational studies to gain further insights into the results obtained. We constructed a biophysically based model of a CA3 network consisting of pyramidal cells (E cells), basket cells (I cells), and O-LM cells (O cells). In the control network model, each E cell spikes sparsely and randomly at low frequency (3.39 ± 0.24 Hz), whereas the E cell population activity exhibits a clear gamma frequency (see Fig. 4*A*). The O cells in the control network spike at theta frequency driven by the E cells, whereas the E cell population interacts with the I cells, generating a weak pyramidal–interneuronal network gamma rhythm (see ref. 28) (Fig. 4*A*). The power spectrum analysis of the model local field potential (LFP) of the control network reflects the distinct spike frequencies of the interneuron types, displaying theta and gamma oscillations (Fig. 4*A*). Next, we changed the parameters of the control network to create an epileptic network. To represent the increase in the pyramidal cell activity, the epileptic network was given an increase in the E cell drive (enough to make the E cells spike at a mean frequency of

NEUROSCIENCE

8.66 ± 0.41 Hz). The Ih maximal conductance of O-LM cells was also reduced by 43% in relation to the control network. These two modifications in the parameters were able to make the O cells spike at most of gamma cycles (Fig. 4*B*). As a consequence, the power spectrum analysis of the model LFP of the epileptic network shows a loss of theta oscillations and an increase in gamma power, without a considerable change in the peak gamma frequency (Fig. 4*B*).

We also simulated the epileptic network without reducing the Ih conductance in O-LM cells, and we observed the same qualitative results as before (data not shown). Moreover, by simulating current clamp experiments in a single O cell, we observed that the increase in the IR induced by lower Ih is not able to compensate for the lower excitability induced by the hyperpolarization of the MP; this is also confirmed by experimental results (see SI Fig. 7) and supported by mathematical analysis of the model (see *SI Appendix 1*). Therefore, these computational studies suggest that the increase in pyramidal cell activity is the critical change accounting for the experimental results obtained.

Discussion

The principal finding of the present study is that hippocampal rhythmogenesis is altered in an animal model of mTLE. In KA-injected mice, theta oscillations are abolished, whereas gamma activity is enhanced both *in vivo* and *in vitro*. O-LM neurons, interneurons critically involved in the generation of theta activity, show an increased excitability, and their discharge frequency shifts from the theta to gamma range during induced network activity *in vitro*. Thus, our results suggest that a change in the activity pattern of a specific type of interneuron leads to loss of a low-frequency network activity in the hippocampus. Altered rhythmogenesis in the hippocampal circuits may in turn underlie the memory problems in mTLE.

Rhythmic oscillatory activity is a hallmark of network function in various brain regions (29). Oscillations arise from synchronized activity of neurons and are thought to play an essential role for information processing in neuronal networks (30, 31). Inhibition and GABAergic interneurons are of critical importance for the generation of both theta and gamma activity (19, 22, 32–35) and for the coordination of the gamma and theta rhythms (36). Dendrite-inhibiting O-LM interneurons play a pivotal role in driving *in vitro* theta oscillations, whereas perisomatic-inhibiting basket cells are important for the generation of gamma activity (19, 37). Theta oscillations have long been implicated in spatial navigation in rodents and humans (14–16). In line with these hypotheses, the loss of hippocampal theta rhythms results in spatial memory deficits with a tight correlation between the degree of memory-task impairment and the reduction in the theta activity (14). Conversely, in $HCN1^{-/-}$ mice, an increased theta activity is associated with an enhanced learning performance in hippocampus-dependent spatial tasks (38).

An impaired spatial performance has also been observed in KA-injected animals (5). It was suggested that the learning and memory deficits in these animals are direct consequences of the epileptic seizures. However, as our experiments revealed a loss of hippocampal theta network oscillations both *in vivo* and *in vitro*, the impairment in hippocampus-dependent tasks may relate to the diminished theta frequency oscillations, rather than to the seizure activity.

Our morphological investigations showed that, in the ventral hippocampus of the KA-injected mice, which is not directly affected by the drug injection, the cellular structure of the hippocampus and the density of somatostatin-immunopositive O-LM interneurons is not changed. Similarly, at the cellular level, morphological analysis of O-LM cells revealed no difference between control and epileptic animals. However, the activity of O-LM interneurons during *in vitro* oscillations was enhanced, and their discharge frequency shifted from the theta to the gamma band. Detailed electrophysiological investigation further showed that the intrinsic properties, including the resting MP, the IR, and the firing properties, differ between these two groups. Additionally, we have found a reduction in Ih. Changes of Ih may not only influence the intrinsic and firing properties but also the synchronization properties of these cells (39, 40). A direct consequence of a reduction in this conductance is an increased IR. The increased IR can facilitate the activation and increase the firing frequency of the neurons. However, impaired Ih shifts the MP to more negative values and therefore may result in lowered excitability. Both a prevalent hyperpolarization and lowered excitability (25) and a dominantly increased IR and increased excitability (41, 42) have been reported previously after the blockade or impairment of the Ih conductance. Our experimental and computational data suggest that, in O-LM cells, the increase in the membrane IR is not able to compensate the MP hyperpolarization, so that impairment in an Ih conductance does not account for the increased firing properties of O-LM cells. Conversely, the reduction of Ih may represent a compensatory mechanism in the mTLE model in response to increased excitatory input (43). Several mechanisms may underlie the Ih reduction, such as a shift in activation curve, a reduced number of channels, and altered cAMP homeostasis (43, 44). Because the voltage sensitivity, kinetics, and sensitivity to cAMP of HCN channels vary with their subunit composition (45), one may argue that alteration in Ih may reflect changes in HCN subunit gene expression (44).

Different possibilities may underlie the observed increases of sEPSCs in O-LM cells from epileptic mice, such as the formation of new functional excitatory synapses, increased probability of synaptic release of glutamate or increased activity of presynaptic pyramidal cells. Indeed, in patients and in experimental models of mTLE, axonal sprouting was associated with the formation of new synapses (46, 47). However, in the same cells, significant reduction in mEPSCs frequency was detected. The decreased frequency of mEPSC suggests a reduction rather than an increase in the number of functional synapses onto ventral O-LM cells in epileptic animals.

Thus, the increased frequency of sEPSCs onto O-LM interneurons is likely to result from an increased activity of presynaptic principal cells in KA-pretreated animals. In fact, our data suggest that, during population activity, *in vitro* pyramidal cell activity is enhanced in these mice as a consequence of reduced firing threshold. Furthermore, our simulations show that the increase in the pyramidal cells activity is a necessary and sufficient factor leading to the enhanced activity of O-LM interneurons during network oscillations. In addition, impairment of the Ih conductance, a conductance that limits the excitatory postsynaptic potential (EPSP) duration (48), will prolong the duration of EPSP and, together with the longer membrane time-constant, may prolong the temporal window for action-potential firing. On a still longer time scale, the experimentally observed persistent increases in excitatory input may have important consequences, limiting the effects of these interneurons in theta generation and nested theta–gamma activity in hippocampal networks.

In summary, the altered firing properties of O-LM cells, in association with their excess excitation and consequently modified dendritic inhibition of principal cells, might lead to the altered network activity observed in both *in vivo* and *in vitro* recordings. Because inhibition-based theta frequency network oscillations are crucially involved in spatial memory, the impaired rhythmogenesis in the hippocampus might contribute to the cognitive and memory deficits in mTLE.

Materials and Methods

Experiments were performed on adult C57/Bl6 mice. All animal procedures were approved by the Regional Berlin Animal Ethics Committee (registration no. T0076/03).

***In Vivo* Experiments.** Mice were stereotaxically injected under general anesthesia (350 mg/kg chloral hydrate i.p.) with either 50 nl of

a 20 mM solution of KA in 0.9% NaCl or the same amount of saline (control mice) into the right CA1 area of the dorsal hippocampus [coordinates: anterior–posterior (AP), −2 mm; medial–lateral (ML), −1.8 mm; dorsal–ventral (DV), −1.6 mm; ref. 49]. Injection was performed for 10 min by using a 0.5-μl microsyringe with stainless steel cannula (outer diameter, 160 μm; Hamilton, Reno, NV) connected to a micropump (UltraMicroPump II; WPI, Sarasota, FL), and the cannula was left in place for an additional 2 min to limit reflux along the cannula track. Field potential recordings were done in the stratum radiatum of the CA3 region of ventral hippocampus (AP, −3.1 mm; ML, −2.6 mm; DV, −3.6 mm) by using mono- or bipolar stainless steel wire electrodes soldered on a male connector (Plastics One, Roanoke, VA).

Field potential recordings were collected in freely moving mice during spontaneous exploration and immobility states in the home cage. All recordings were performed at 3–4 weeks after KA-injection (30–60 min/day for 6–8 days) in the chronic phase. Recordings were low-pass filtered at 1 kHz with a custom-made Bessel filter, digitized at 2 kHz by using an ITC-16 A/D board (Instrutech, Mineola, NY), and analyzed using WinTida software (Heka, Lambrecht, Germany). Upon completion of the experiments, histological analysis was performed in all mice after Cresyl violet staining to verify the site of the KA injection, the location of recording electrodes and the typical dispersion of dentate gyrus granule cells (see 6).

In Vitro* Experiments.** ***Slice preparation. Coronal slices (450-μm thickness) were obtained from ventral hippocampus of control and KA-treated mice. Slices were incubated at room temperature for at least 1 h in a holding chamber and then were transferred to the recording chamber. The solution used during incubation and recording contained 126 mM NaCl, 3 mM KCl, 1.25 mM NaH_2PO_4, 2 mM $CaCl_2$, 2 mM $MgSO_4$, 24 mM $NaHCO_3$, and 10 mM glucose saturated with 95% O_2 and 5% CO_2.

Extracellular field recordings were similar to those described in Gloveli *et al.* (22). Detailed information about the whole-cell recordings and measurements of the intrinsic and synaptic properties can be found in *SI Methods*.

Immunohistochemistry. The slices from KA-treated mice containing the dorsal and ventral hippocampus were collected after experiments for immunohistochemistry (see *SI Methods*).

Anatomical Identification of Biocytin-Filled Interneurons. Slices with a biocytin-filled interneuron were processed as described in ref. 19. Subsequently, the cells were reconstructed with the aid of a Neurolucida 3D reconstruction system (MicroBrightField, Williston, VT).

Modeling and Simulations. We used a five-compartment model for the pyramidal cell (E cell) and single compartment models for the O-LM (O) and basket (I) cells (36). All cells were modeled by using the Hodgkin–Huxley formalism. The model CA3 network consisted of 40 E, 5 I, and 5 O cells. In the network, the synapses were all-to-all, and the following connections were modeled: E–I, E–O, I–I, I–E, I–O, O–E, and O–I. I cells synapse on the somatic compartment of E cells, whereas O cells synapse on the distal apical dendritic compartment of E cells. Detailed information about the model cells and synapses, the model LFP, and numeric and random aspects of this work can be found in *SI Appendix 2*. The model LFPs were subjected to power spectrum analyses by using standard routines in MATLAB software. All simulations were carried out using the NEURON simulation program (50).

We thank Prof. R. D. Traub for helpful discussions and S. Ferl for technical assistance. This study was supported by Sonderforschungsbereich Grant TR3/B5 and European Union Grant FP6 EPICURE (to T.G., T.D., I.V. and U.H.), National Institutes of Health Grant R01 NS46058 as part of the National Science Foundation/National Institutes of Health Collaborative Research in Computational Neuroscience Program (to N.J.K.), and Conselho Nacional de Desenvolvimento Cientifico e Tecnologico (Brazil) Grant 201038/2005-6 (to A.B.T.).

1. Engel J (2001) *Neuroscientist* 7:340–352.
2. Holmes GL, Thompson JL, Marchi T, Feldman DS (1988) *Epilepsia* 29:721–730.
3. Breier JI, Plenger PM, Wheless JW, Thomas AB, Brookshire BL, Durtis VL, Paranicolaou A, Willmore LJ, Clifton GL (1996) *Epilepsia* 3:165–170.
4. Yin S, Guan Z, Tang Y, Zhao J, Hong J, Zhang W (2005) *Brain Res* 1053:195–202.
5. Stafstrom CE, Chronopoulos A, Thurber S, Thompson JL, Holmes GL (1993) *Epilepsia* 34:420–432.
6. Bouilleret V, Ridoux V, Depaulis A, Marescaux C, Nehlig A, Le Gal La Salle G (1999) *Neuroscience* 89:717–729.
7. Sayin U, Sutula TP, Stafstrom CE (2004) *Epilepsia* 45:1539–1548.
8. Bouilleret V, Loup F, Kiener T, Marescaux C, Fritschy JM (2000) *Hippocampus* 10:305–324.
9. Straessle A, Loup F, Arabadzisz D, Ohning GV, Fritschy JM (2003) *Eur J Neurosci* 18:2213–2226.
10. Magloczky Z, Freund TF (2005) *Trends Neurosci* 28:334–340.
11. Cossart R, Dinocourt C, Hirsch JC, Merchan-Perez A, De Felipe J, Ben-Ari Y, Esclapez M, Bernard C (2001) *Nat Neurosci* 4:52–62.
12. Wittner L, Eross L, Czirjak S, Halasz P, Freund TF, Magloczky Z (2005) *Brain* 128:138–152.
13. White JA, Banks MI, Pearce RA, Kopell NJ (2000) *Proc Natl Acad Sci USA* 97:8128–8133.
14. Winson J (1978) *Science* 201:160–163.
15. O'Keefe J, Recce M (1993) *Hippocampus* 3:317–330.
16. Kahana MJ, Sekuler R, Caplan JB, Kirschen M, Madsen JR (1999) *Nature* 399:781–784.
17. Hasselmo ME (2005) *Hippocampus* 15:936–949.
18. Arabadzisz D, Antal K, Parpan F, Emri Z, Fritschy JM (2005) *Exp Neurol* 194:76–90.
19. Gloveli T, Dugladze T, Saha S, Monyer H, Heinemann U, Traub RD, Whittington MA, Buhl EH (2005) *J Physiol* 562:131–147.
20. Heinrich C, Nitta N, Flubacher A, Muller M, Fahrner A, Kirsch M, Freiman T, Suzuki F, Depaulis A, Frotscher M, Haas CA (2006) *J Neurosci* 26:4701–4713.
21. Bragin A, Jando G, Nadasdy Z, Hetke J, Wise K, Buzsaki G (1995) *J Neurosci* 15:47–60.
22. Gloveli T, Dugladze T, Rotstein HG, Traub RD, Monyer H, Heinemann U, Whittington MA, Kopell NJ (2005) *Proc Natl Acad Sci USA* 102:13295–13300.
23. Gillies MJ, Traub RD, LeBeau FE, Davies CH, Gloveli T, Buhl EH, Whittington MA (2002) *J Physiol* 543:779–793.
24. Pike FG, Goddard RS, Suckling JM, Ganter P, Kasthuri N, Paulsen O (2000) *J Physiol* 529:205–213.
25. Maccaferri G, McBain CJ (1996) *J Physiol* 497:119–130.
26. Saraga F, Wu CP, Zhang L, Skinner FK (2003) *J Physiol* 552:673–689.
27. Blasco-Ibanez JM, Freund TF (1995) *Eur J Neurosci* 7:2170–2180.
28. Börgers C, Epstein S, Kopell NJ (2005) *Proc Natl Acad Sci USA* 102:7002–7007.
29. Buzsaki G, Draguhn A (2004) *Science* 304:1926–1929.
30. Buzsaki G, Chrobak JJ (1995) *Curr Opin Neurobiol* 5:504–510.
31. Singer W, Gray CM (1995) *Annu Rev Neurosci* 18:555–586.
32. Cobb SR, Buhl EH, Halasy K, Paulsen O, Somogyi P (1995) *Nature* 378:75–78.
33. Whittington MA, Traub RD, Jefferys JG (1995) *Nature* 373:612–615.
34. Bartos M, Vida I, Frotscher M, Meyer A, Monyer H, Geiger JR, Jonas P (2002) *Proc Natl Acad Sci USA* 99:13222–13227.
35. Whittington MA, Traub RD (2003) *Trends Neurosci* 26:676–682.
36. Tort ABL, Rotstein HG, Dugladze T, Gloveli T, Kopell NJ (2007) *Proc Natl Acad Sci USA* 104:13490–13495.
37. Mann EO, Suckling JM, Hajos N, Greenfield SA, Paulsen O (2005) *Neuron* 45:105–117.
38. Nolan MF, Malleret G, Dudman JT, Buhl DL, Santoro B, Gibbs B, Vranskaya S, Buzsaki G, Siegelbaum SA, Kandel ER, Morozov A (2004) *Cell* 119:719–732.
39. Acker CD, Kopell N, White JA (2003) *J Comput Neurosci* 15:71–90.
40. Rotstein HG, Pervouchine DD, Acker CD, Gillies MJ, White JA, Buhl EH, Whittington MA, Kopell N (2005) *J Neurophysiol* 94:1509–1518.
41. Strauss U, Kole MH, Brauer AU, Pahnke J, Bajorat R, Rolfs A, Nitsch R, Deisz RA (2004) *Eur J Neurosci* 19:3048–3058.
42. Kole MH, Brauer AU, Stuart GJ (2007) *J Physiol* 578:507–525.
43. Chen K, Aradi I, Santhakumar V, Soltesz I (2002) *Trends Neurosci* 23:552–557.
44. Chen K, Aradi I, Thon N, Eghbal-Ahmadi M, Baram TZ, Soltesz I (2001) *Nat Med* 7:331–337.
45. Robinson RB, Siegelbaum SA (2003) *Annu Rev Physiol* 65:453–480.
46. Esclapez M, Hirsch JC, Ben-Ari Y, Bernard C (1999) *J Comp Neurol* 408:449–460.
47. Houser CR (1999) *Adv Neurol* 79:743–761.
48. Yamada R, Kuba H, Ishii TM, Ohmori H (2005) *J Neurosci* 25:8867–8877.
49. Paxinos G, Franklin KBJ (2001) *The Mouse Brain in Stereotaxic Coordinates* (Academic, San Diego), 2nd Ed.
50. Hines ML, Carnevale NT (1997) *Neural Comput* 9:1179–1209.